Journal of the European Ceramic Society **13** (1994) 345–353

Transmission Electron Microscopy Studies of AlN Deposits

D. Dorignac, A. Mazel, Y. Kihn, J. Sévely

CNRS/CEMES-LOE, BP 4347, 31055 Toulouse, France

B. Aspar, B. Armas & C. Combescure

CNRS/IMP, BP 5, Odeillo-Font-Romeu, France

(Received 5 July 1993; revised version received 22 November 1993; accepted 25 November 1993)

Abstract

AlN deposits, prepared by low-pressure chemical vapour deposition (LPCVD), with or without N_2O addition in the source gases, have been examined by several complementary transmission electron microscopy (TEM) techniques, including electron diffraction (ED), high-resolution electron microscopy (HREM), electron energy loss and extended energy loss fine structure spectroscopies (EELS and EXELFS), to determine both the structures and local chemical compositions.

The major differences between the compounds lie in the occurrence of micro- and nanostructural changes, as dendrites and extended defects. It is suggested that the observed structural changes are induced by oxygen impurities. The implications of the results for the interpretation of some physical properties of the compounds are discussed in terms of these changes.

Mit Hilfe von verschiedenen komplementären Techniken im Rahmen der Transmissions-Elektronenmikroskopie (TEM), Elektronenbeugung (ED), Hochauflösungsmikroskopie (HREM) und Energieverlustspektroskopie (EELS und EXELFS) werden durch LPCVD vorbereitete AlN-Rückstände, mit oder Zugabe von N_2O in die Quellengase untersucht, um sowohl ihre Struktur als auch ihre lokalechemische Zusammensetzung zu bestimmen.

Die Hauptunterschiede zwischen den beiden Typen von Verbindungen bestehen in der Veränderung von Mikro- und Nano-struktur, wie z.B. das Auftreten von Dendriten und weitreichenden Defekten. Es ist anzunehmen, daß diese Strukturveränderungen von Sauerstoffunreinheiten hervorgerufen werden. Desweiteren wird untersucht, wie sich diese Strukturveränderungen auf die Interpretation einiger physikalischer Eigenschaften dieser Verbindungen auswirken.

Des dépôts d'AlN préparés par LPCVD, avec ou sans addition de N_2O dans les gaz vecteurs, ont été examinés au moyen de plusieurs techniques complémentaires de microscopie électronique par transmission (TEM), notamment la diffraction électronique (ED), la microscopie électronique à haute résolution (HREM) et la spectroscopie des pertes d'énergie (EELS et EXELFS), afin de déterminer à la fois leurs structures et leurs compositions chimiques locales.

Les différences majeures entre ces deux types de composés résident dans des changements de micro- et de nano-structure, comme l'apparition de dendrites et de défauts étendus. On est en droit de penser que ces changements de structure sont induits par des 'impuretés' d'oxygène. On examine aussi les répercussions que ces changements de structure peuvent avoir quant à l'interprétation de quelques unes des propriétés physiques de ces composés.

1 Introduction

Aluminium nitride (AlN) coatings obtained by low-pressure chemical vapour deposition (LPCVD) are of considerable interest in advanced material sciences, since they have important potential applications, particularly as electronic substrates, refractory materials and high-temperature oxidation-resistant compounds. Moreover, as already widely discussed, their physical properties are known to be strongly dependent on the microstructure and, therefore, on the processing parameters.

A first approach to obtaining information on the microstructure and surface morphology of the deposits was by the use of X-ray diffraction (XRD) and scanning electron microscopy (SEM) techniques.[1,2] It has been suggested that the compounds could be stabilized against hydrolysis by incorporating a small quantity of oxygen.

Journal of the European Ceramic Society 0955-2219/94/$7.00

The present work is thus primarily concerned with establishing the influence of oxygen on microcrystal growth and on local structure at an atomic level. The experimental applicability of the TEM techniques to the study of these coatings is also demonstrated, together with the details of microcrystal shapes and sizes, chemical compositions and nanostructures, shown by the results.

2 Experimental

2.1 Chemistry

LPCVD is one of the most attractive techniques for producing AlN coatings because they are directly obtained by thermal decomposition of raw vapours or gases. The experimental device used for the elaboration of the samples is described by Aspar.[2] It consists of a vertical hot-wall reactor composed of a graphite susceptor heated by high-frequency induction. The temperature is measured using an optical micropyrometer.

In the present experiments, the source gases were hydrogen (H_2), ammonia (NH_3), nitrogen (N_2) with or without nitrous oxide (N_2O). The aluminium source, aluminium chloride vapour ($AlCl_3$), was supplied by evaporation of solid $AlCl_3$ at 80°C and carried by N_2. The $AlCl_3$ vapour and the NH_3 gas, both diluted with N_2, were introduced separately in the reaction zone to avoid the formation of complexes.[3] The substrates consisted of graphite coated with a CVD-deposited SiC layer.

The standard AlN deposition parameters were: total pressure 130 Pa, substrate temperature 1000°C, and experimental ratios $AlCl_3/NH_3 = 2$ and $N_2/AlCl_3 = 200$. For AlN deposits prepared by progressively introducing N_2O in the gas mixture, identical total pressure and substrate temperature, but different experimental ratios, $AlCl_3/NH_3 = 1{\cdot}35$, $N_2O/AlCl_3 = 15{\cdot}5$, $H_2/NH_3 = 10$ and $N_2/N_2O = 17{\cdot}6$ were used. Henceforward, these two kinds of compounds will be referred as 'pure' AlN and as 'oxygen-doped' AlN, respectively.

2.2 Electron microscopy

Thin specimens, adequate for electron microscopy, were then prepared from the above samples by mechanical polishing and by Ar^+ ion milling at liquid N_2 temperature. An operating difficulty, characteristic of most ceramics, which is that electrostatic charging effects under the electron beam of the microscope may occur, has been overcome by carefully pasting the specimens onto the supporting copper grids with droplets of silver lacquer.

The electron microscope used was a Philips (CM30ST), operating at 300 kV, with a point resolution of 0·20 nm (i.e. the first zero cross-over in the microscope transfer function for the optimum defocus value, −58 nm, corresponding to the minimum size of the object details whose images are directly interpretable).

For TEM and ED, standard bright-field (BF) and dark-field (DF) procedures were used, with magnifications and camera lengths of about 50 k and 930 mm, respectively.

For HREM, a careful operating procedure was followed at direct magnification of 1M in the axial-illumination bright-field (AIBF) mode, via a Sofretec (CF1500) high-resolution TV camera, for image acquisition, and a Synoptics advanced software package (SysTEM), for microscope control and on-line image processing, namely: (i) fine astigmatism correction, (ii) accurate coma-free alignment, and (iii) identification of the zero-contrast focus position, using ultra-thin amorphous regions adjacent to the areas of interest. The experimental images and the corresponding digitized diffractograms were examined on a TV screen with about 18M magnification and on a high-definition (1024 × 768) RGB monitor screen, respectively. The simulated images were computed using standard (MacTEMPAS[4]) multislice techniques, since no additional improvement is really needed for relatively simple structures consisting of low-Z elements,[5] such as those investigated here.

2.3 Electron spectroscopy

For EELS, an on-line Gatan (666) parallel detector spectrometer, with an attainable energy resolution of 1·5 eV (full width at half maximum of the zero-loss peak), was used. Appropriate electron probe diameters, varying from 10 to about 40 nm, were chosen.

For the quantitative chemical analyses the EELS spectra were processed using standard Gatan software. For analysing the EXELFS modulations a software developed in the laboratory was used.[6]

3 Results

3.1 'Pure' AlN

Figures 1(a) and 1(b) show low-magnification TEM BF (bright-field) and DF (dark-field) pictures which are typical of the general aspect of the samples elaborated without N_2O. The material consists of a juxtaposition of microcrystals. In the areas of large thickness, some continuous contrast lines, which are frequently angular, indicate probable crossed crystals. On the border of the specimen holes (bottom of the figures), where thinner microcrystals are located, the average microcrystal size is of the order of 2 to 3 μm.

The selected-area ED pattern, shown in the inset,

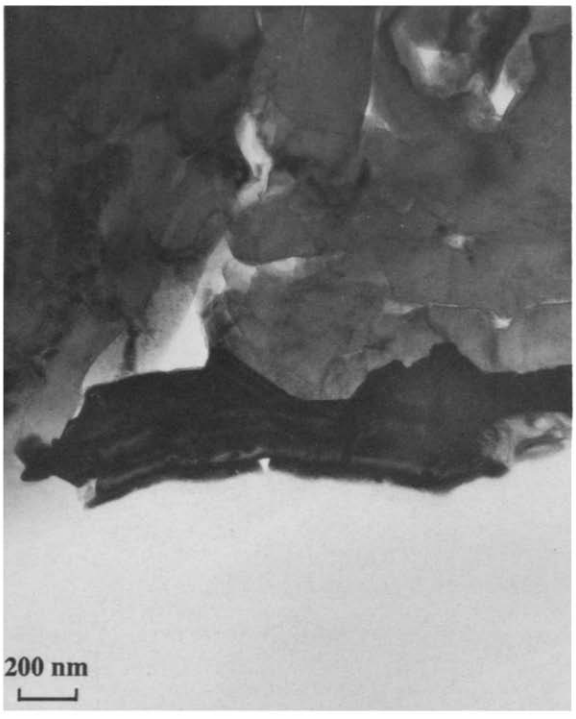

(a)

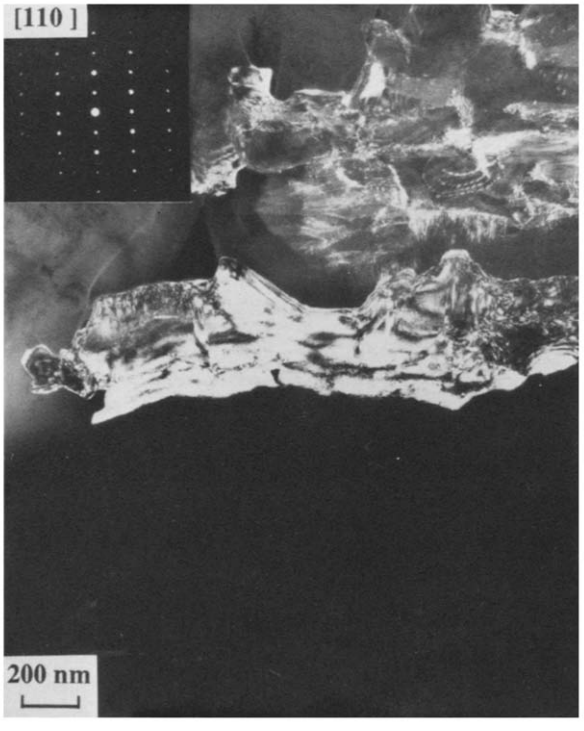

(b)

Fig. 1. Low-magnification TEM (a) bright-field and (b) dark-field images illustrating the microcrystalline structure of the 'pure' AlN coatings. Note the average microcrystal size of the order of 2 to 3 μm. The inserted ED pattern, for $\langle 110 \rangle$ zone axis, confirms the normal AlN wurtzite 2H-type crystalline structure.

corresponds to one of these microcrystals, well oriented along the $\langle 110 \rangle$ direction. It indicates without any ambiguity that the observed structure corresponds to the wurtzite 2H-type crystalline structure of the pure AlN.[7] The three-dimensional unit cell model and the corresponding two-dimensional $\langle 110 \rangle$ projection are given in Fig. 2.

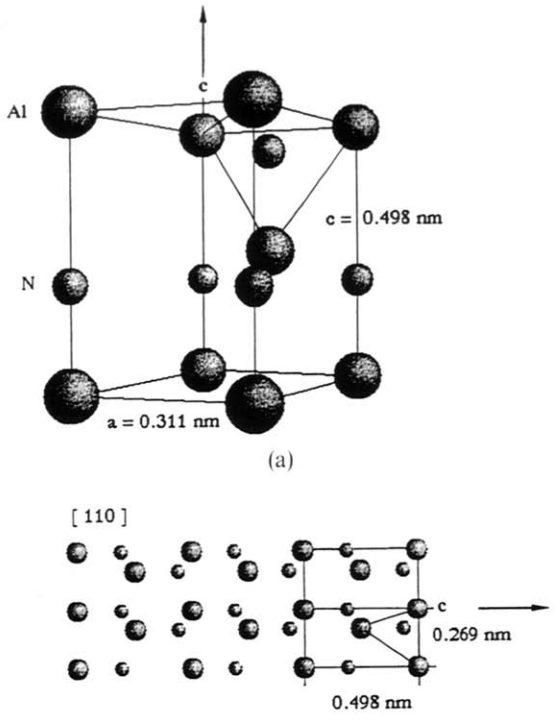

Fig. 2. Perspective view of the AlN wurtzite unit cell and the corresponding $\langle 110 \rangle$ projected structure.

This structure is clearly visible in the AIBF HREM images shown in Fig. 3. The two pictures correspond to the same specimen area, a very thin edge having a uniform thickness of about 5 nm (the amorphous part corresponding to the border of an adjacent hole can be seen in the top of the pictures), but observed with different defoci, -113 nm and -89 nm, respectively. According to the very good image match with the computer-image simulations, shown in the insets together with the projected atomic potentials, the atomic columns are known to appear with 'black' or 'white' contrast, for these values of defocus. Note that, in fact, the limited microscope resolution does not permit the 0·106 nm projected Al–N distance to be resolved, but only the distance between two neighbouring (Al–N) bi-columns, which is 0·265 nm (cf. Fig. 8).

Figure 4 shows another high-magnification HREM image displaying features common to most of the images recorded. It corresponds to a 'wedge-shaped' microcrystal. The crystal thickness, which increases progressively from top to bottom, can easily be determined by image matching with simulations for the chosen defocus, -90 nm. Three examples, corresponding to thicknesses of about 10, 12 and 15 nm, are inserted. Note that the true $\langle 110 \rangle$ projected structure is recognizable only very close to the thin edge (within 1 to 5 nm). Elsewhere the image becomes more and more complicated throughout the remainder of the field, with also sharp variations in contrast, including reversals from black to white. However, the image symmetry, expected from the

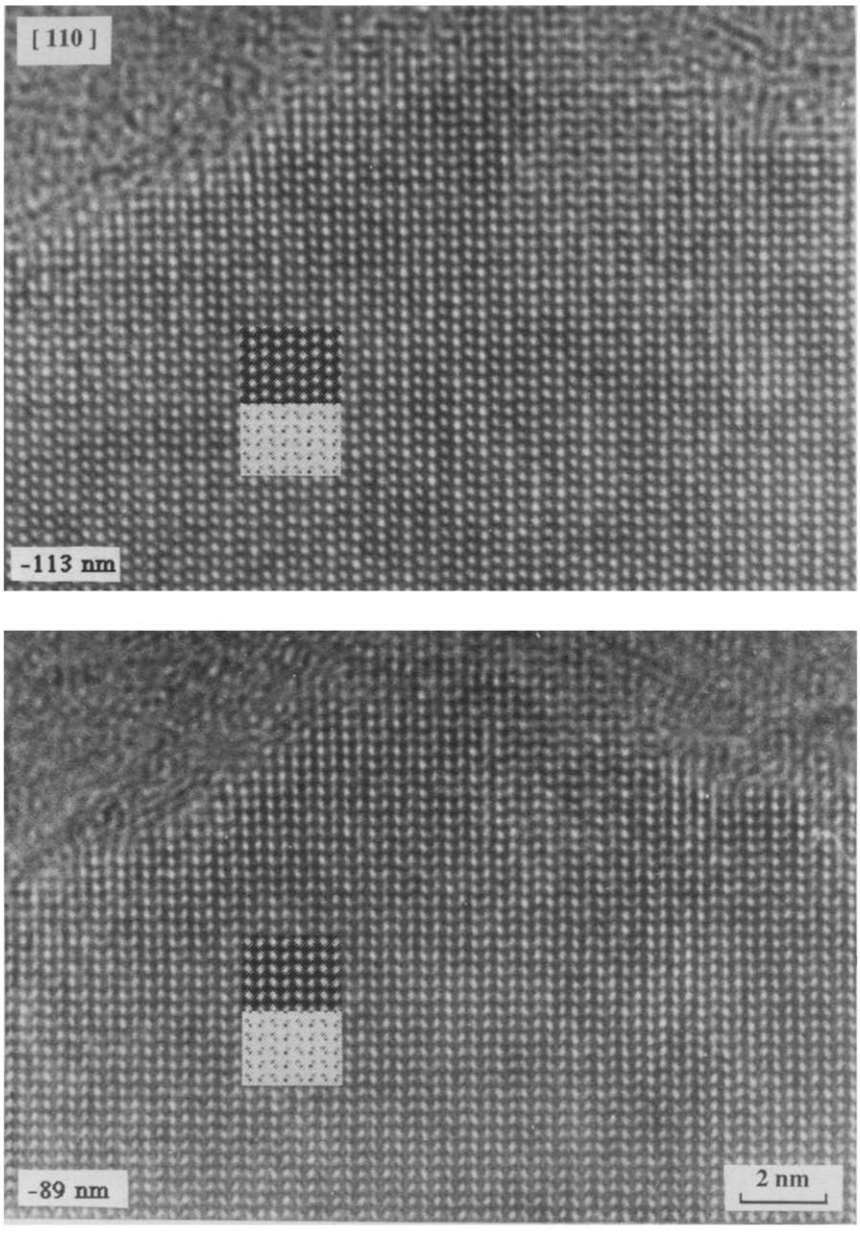

Fig. 3. Axial-illumination bright-field HREM images of a 'pure' AlN microcrystal with uniform thickness, observed in ⟨110⟩ direction. The corresponding atomic projected potentials and image simulations, for the two indicated defoci, clearly reveal the wurtzite structure (top: 'black' atoms; bottom: 'white' atoms).

wurtzite 2H-type structure (space group $P6_3mc$), is conserved.

Figure 5 shows typical examples of EELS spectra obtained from individual microcrystals and exhibiting the characteristic N– and Al–K edges at 400 eV and 1560 eV, respectively. The deduced N/Al atomic concentration ratio is $1 \mp 0{\cdot}05$, in agreement with both the AlN chemical stoichiometry and the wurtzite crystalline structure.

3.2 'Oxygen-doped' AlN

Figure 6(a) shows a low magnification TEM BF picture typical of most of the samples prepared with a N_2O gas flow. The material appears to consist of a disordered assembly of similar microcrystals, having a planar random arrangement parallel to the surface plane of the coating (here, the observation plane) and exhibiting 'feather-like' shapes, with an average size of about 1 μm × 100 nm.

Intermediate magnification pictures, see Fig. 6(b), reveal the presence of dendrites, appearing on both sides of more homogeneous central zones. However, dendrites are not visible in the crystal tips. This is shown in Fig. 7, which shows examples of TEM DF images obtained by selecting the 1–11 diffraction spot, the incident electron beam direction being parallel to the ⟨110⟩ zone axis. The associated ED pattern, where the −11–1, 1–11 and 2–22 reflections appear amongst the more intense, is inserted. As for 'pure' AlN, such ED patterns also confirm the wurtzite 2H-type crystalline structure. The projection of the c axis onto the image plane is in this case

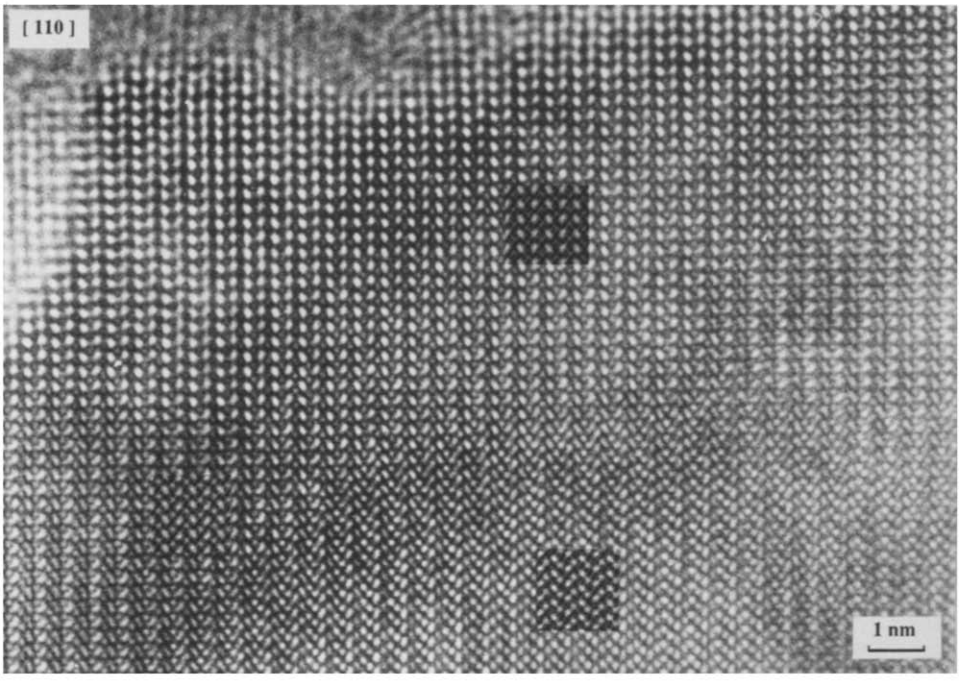

Fig. 4. High-magnification HREM image of a 'wedge-shaped' 'pure' AlN microcrystal. Note the image changes when the crystal thickness is progressively increasing, from top to bottom, in perfect agreement with the (inserted) computer simulations for the ⟨110⟩ projected wurtzite structure.

parallel to the direction of the dendrites, demonstrating that they are generated by growth of the (001) planes.

Figure 7 likewise shows another characteristic typical of the observed images, where a straight line appears across the central part of the microcrystals and generally persists to their extremities (another example of this type of microcrystals can also be s.

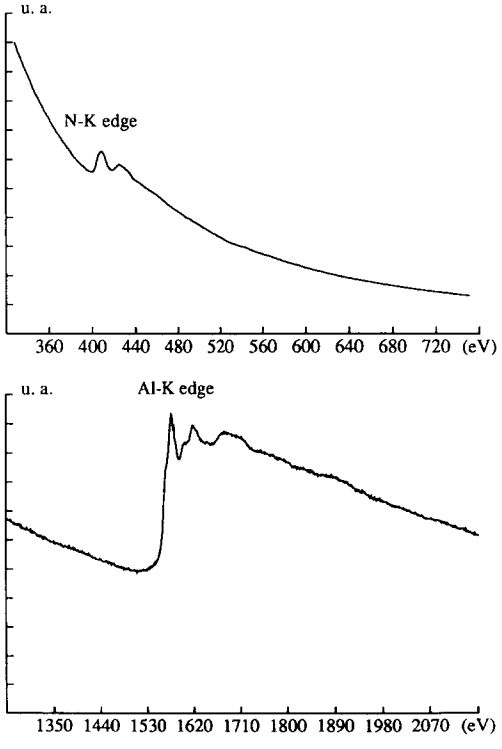

Fig. 5. Typical EELS spectra obtained from 'pure' AlN microcrystals. Their quantitative analysis, which leads to the atomic concentration ratio (N/Al) = $1 \mp 0{\cdot}05$, confirms that the material is stoichiometric.

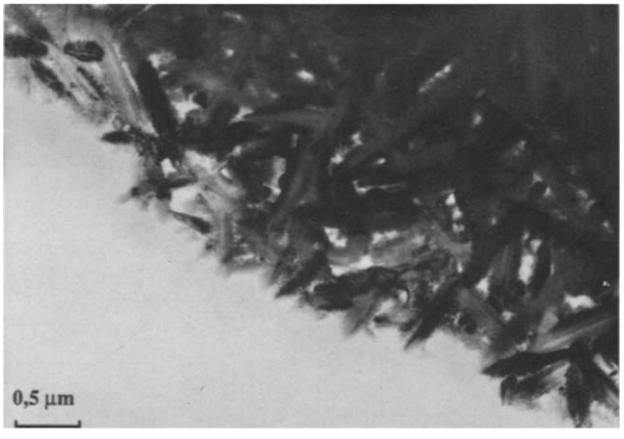

(a)

(b)

Fig. 6. Low-magnification (a) and intermediate-magnification (b) bright-field TEM images showing the microcrystalline structure of the 'oxygen-doped' AlN coatings. Note the characteristic 'feather-like' morphology of the microcrystals, with an average size of about 1 μm × 100 nm. Note also the occurrence of lateral dendrites and, sometimes, of central extended defects (top-left corner).

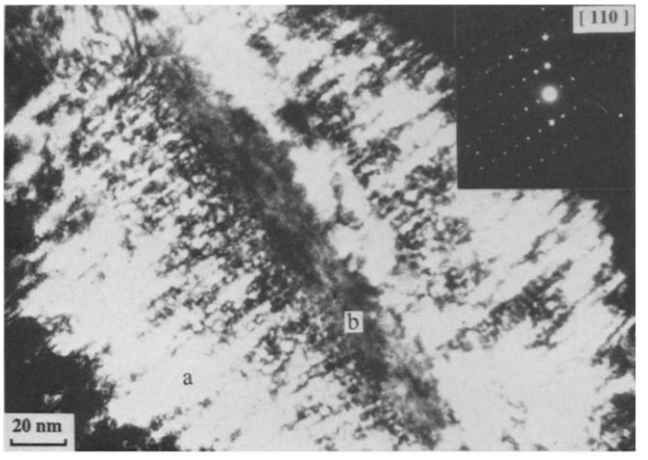

(a)

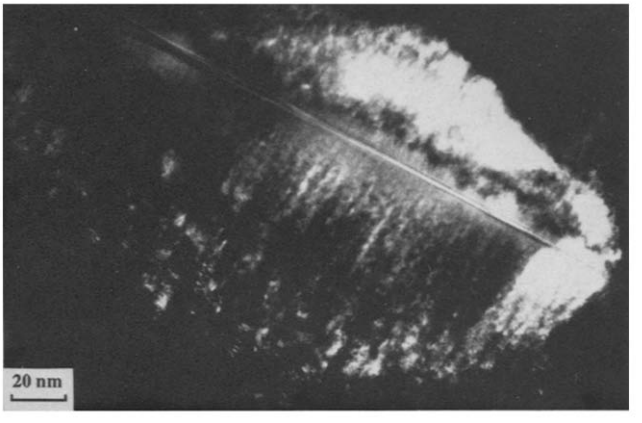

(b)

Fig. 7. TEM dark-field images illustrating the 'dendritic' aspect of the 'oxygen-doped' AlN microcrystals, (a) without or (b) with the presence of a central extended defect.

in the top-left corner of Fig. 6(b)). Such high-contrast lines indicate the presence of isolated and extended structural defects.

When examined in the HREM mode, the parts confined to the thin edges are revealed to be constituted by parallel stacking faults. A typical example is given in Fig. 8 where the bottom extremity of the defect shown in Fig. 7 is seen. It is clear that in the thinnest region, near the amorphous part, atomic shifts occurred in two particular (001) atomic planes. From the simulated images (for a microscope defocus of -58 nm and a crystal thickness of 4 nm, giving rise to 'black' atoms) the atomic displacements can be determined accurately and the defect can easily be identified as two intrinsic (I1 type) stacking faults, separated by eleven intermediate (001) planes. The corresponding projected structural model is shown in the inset.

Figure 9 shows examples of the correlative characteristic EELS spectra, corresponding either to the outer (a) or to the inner (b) parts of the microcrystals. The observed differences mainly concern the O–K edge intensity distribution at 532 eV, which is just sufficient for reliable quantitative analysis. They reveal O/N atomic concentration ratios about two times higher for (a) than for (b), that is $0{\cdot}7 \pm 0{\cdot}05$ and $0{\cdot}4 \mp 0{\cdot}05$, respectively, while the corresponding N/Al ratios remain equal to $1 \mp 0{\cdot}05$, as for the 'pure' AlN compound. It should be noted that these average values, deduced from systematic studies on several microcrystals, correspond to sample thicknesses

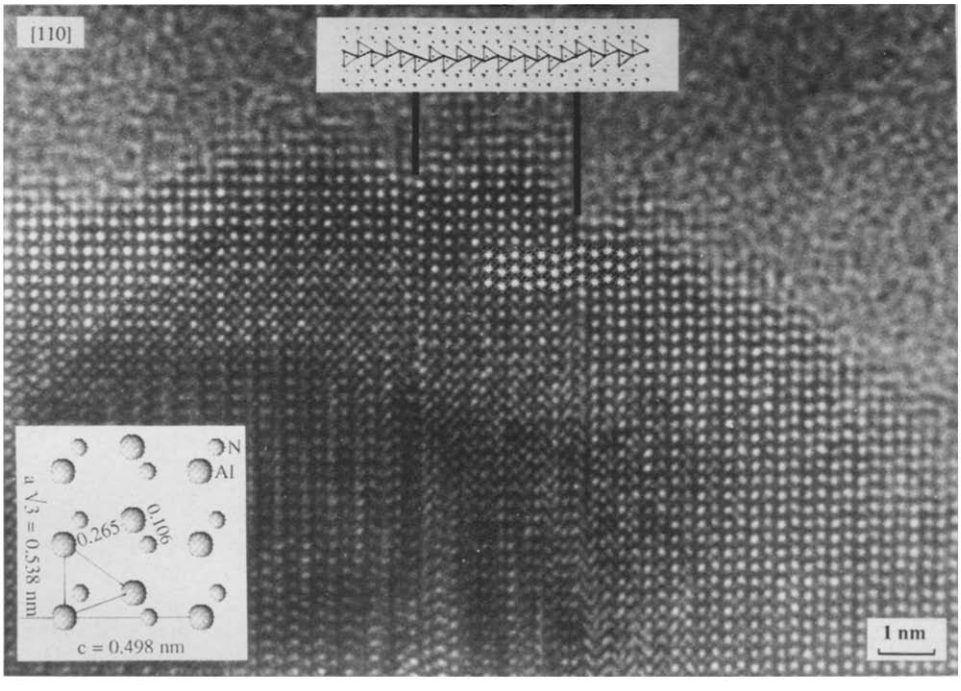

Fig. 8. Axial-illumination bright-field HREM image corresponding to the bottom right extremity of the central defect shown in Fig. 7(b). From the simulations ('black' atoms) the defect is revealed to be a double intrinsic stacking fault (I1 type). The corresponding structural model is inserted at the top.

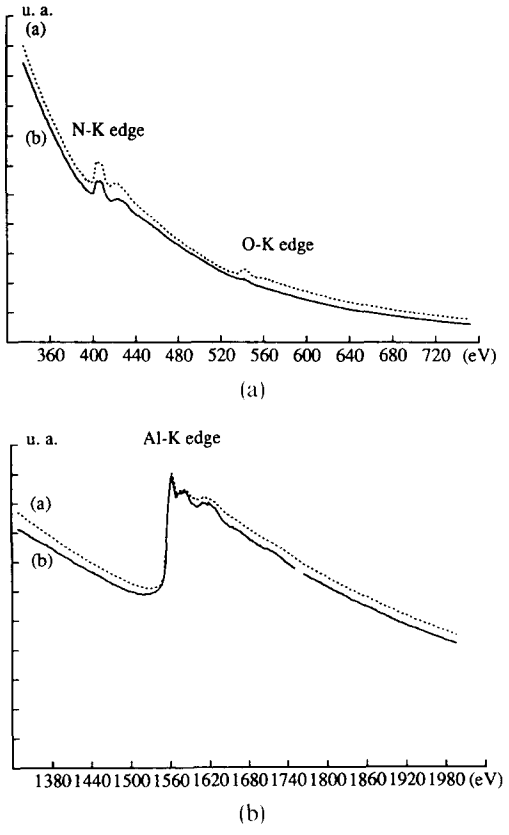

Fig. 9. Typical EELS spectra obtained from the lateral (a) and the central (b) parts of the 'oxygen-doped' AlN microcrystals. Their analyses indicate O/N atomic concentration ratios about two times higher for (a) than for (b).

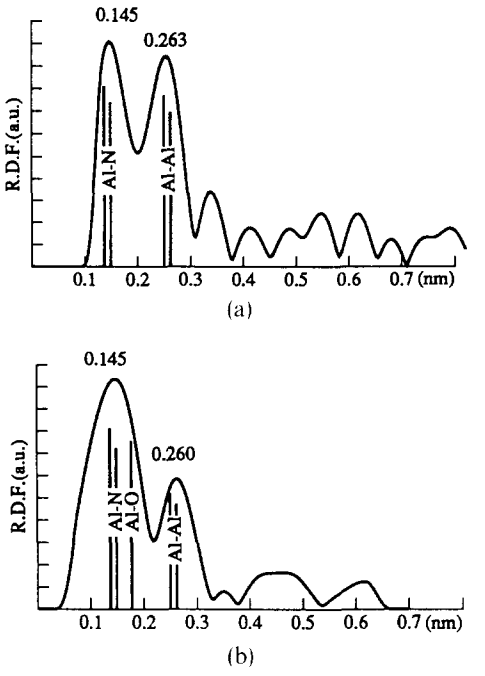

Fig. 10. Typical RDFs obtained from the EXELFS modulations around the Al–K edges, for (a) 'pure' and (b) 'oxygen-doped' AlN compounds. The enlargement of the first main peak reveals that single O atoms are inserted in the wurtzite AlN unit cells.

much smaller than the plasmon mean free path for inelastic scattering. They will not be affected by a possible thickness effect on the EELS spectra,[8] which would further decrease the O/N ratios in the inner (i.e. thicker) (b) parts of the microcrystals. They indicate that oxygen is mainly concentrated in the dendrites and also that it certainly does not replace the N atoms in the crystalline lattice.

To clarify this last point, the EXELFS amplitude oscillations, which appear in a small range of spatial frequencies just above the Al–K edges, have been analysed. The analysis is based on the fact that the one-dimensional inverse Fourier transform of the EXELFS reciprocal-space oscillations is qualitatively similar to the real-space radial distribution function (RDF) of the atoms in the neighbourhood of the Al atoms. As an example, Fig. 10 shows the RDFs resulting from the spectra given in Fig. 5, for pure AlN, and Fig. 9 (curve (a)), for oxygen-doped AlN. In both curves, two analogous main peaks can be identified after a 0·047 nm phase shift correction: the first, at 0·145 nm, corresponds to the combination of the two Al–N distances (0·1885 nm and 0·1916 nm), while the second, around 0·260 nm, corresponds to the combination of the two Al–Al distances (0·3069 nm and 0·3111 nm). But for the oxygen-doped AlN, an appreciable enlargement of the first peak can be seen, which can only be attributed to the additional Al–O distance (0·2185 nm) corresponding to O atoms filling the empty octahedral sites of the hexagonal-close-packed structure. This clearly demonstrates that the O atoms can be in insertion in the crystalline lattice, as previously proposed by Hagège & Ishida.[9]

4 Discussion

The present results reflect the morphological changes and the different microstructures, nanostructures and local chemical compositions existing in the microcrystals constituting the 'pure' and the 'oxygen-doped' AlN coatings. The 'pure' AlN microcrystals were generally found to be relatively homogeneous, with the expected AlN wurtzite crystalline structure and with practically no defects. In contrast, the 'oxygen-doped' AlN microcrystals systematically showed inhomogeneities as dendrites located in their lateral parts. Moreover, their nanostructure appeared very dependent upon the observed microcrystals, a large part of them exhibiting central defects, the length of which usually extended over the whole microcrystals. The most structurally important feature of the observed defects lies in their 'single intrinsic stacking fault' structure, at least as observed at the ultrathin extremities of the microcrystals. Elsewhere, of course, the crystals are generally rather thicker than ideal and the HREM imaging is impossible, even for incident electrons with 300 keV kinetic energy.

The question of the influence of the oxygen on the occurrence of both the dendrites and the extended

defects now arises. Concerning the dendrites, it is known from the EELS and EXELFS results that they certainly contain oxygen atoms in insertion in the crystalline lattice and, as demonstrated by ED results, that they are generated by the growing of the (001) planes. Taking into account the hydrogen blocking effect on the development of these (001) faces,[10] it can therefore be concluded that the formation of the dendrites is very probably a consequence of oxygen–hydrogen chemical reactions, which could appreciably reduce the blocking effect. The resulting O atoms in the structure could then be distributed more or less homogeneously within the dendrites.

Concerning the isolated defects, the basic question is again the following: how do these defects form when the microcrystals are growing, and do they contain oxygen atoms? Because of their absence in the pure AlN microcrystals and, in contrast, their abundance in the oxygen-doped AlN microcrystals, it is probable that these defects could have been created, like the dendrites, during the progressive introduction of N_2O in the gas mixture used as a precursor. This has to be correlated with the fact that other AlN defect structures are known to have a large affinity for oxygen as an impurity.[11–13] These chemically induced stacking faults could also have been capable of progressively accommodating single O atoms, one per original unit cell, in agreement with the average EELS and EXELFS results found in the central regions where they are located. It should then be possible that oxygen atoms remain locally concentrated in the corresponding basal planes. However, it is unfortunately not yet possible to prove this by means of EELS spectroscopy, since the local detection of small amounts of such light atoms is not feasible at present. Moreover, till now, no experimental evidence of this has been obtained by means of HREM imaging, although the presence of the O atoms can modify the image contrast, just sufficiently to be noted. See, for example, the comparative simulations shown in Fig. 11, which emphasize that O atoms are not present in the stacking faults shown in Fig. 8. Another possible explanation is that the O atoms may rapidly be evacuated during their observation under the electron beam, particularly in the ultrathin areas required for HREM. Extensive HREM observations are in progress to clarify these points.

5 Concluding Remarks

Thus a new insight is gained into the structural changes that may accompany the elaboration of some AlN coatings.

The consequences of these features are certainly important in understanding the behaviour of these materials. Their physical characteristics may effectively depend upon the dendrite distribution, for example, or upon the defect size, and in particular upon the ease with which they can deform in response to high mechanical stresses or to high temperatures.

In conclusion, it is pointed out that this work was intended not only to give useful information for chemists and physicists involved in ceramics research but also to illustrate the power of HREM combined with ED, EELS and EXELFS for studying, at the atomic level, the nanostructure of a wide range of analogous materials. The authors are currently performing similar studies on SiC compounds.[14] The authors would also emphasize that the actual limitations of the methodologies will soon be overcome with the availability of the next generation of very high-resolution electron microscopes, with point resolutions well below 0·2 nm, and equipped with highly coherent field-emission guns, permitting much smaller probes to be formed.

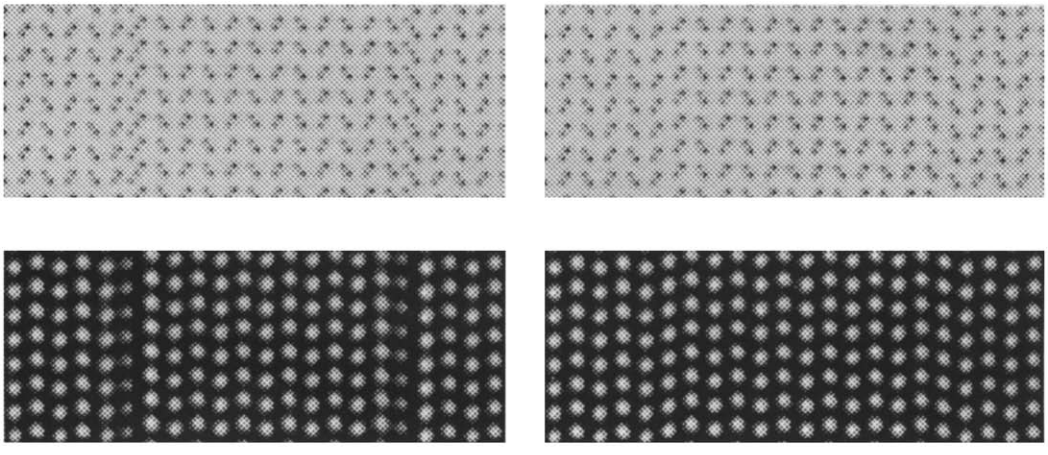

Fig. 11. HREM computer-image simulations (bottom) and corresponding projected-structure potentials (top), with (left) or without (right) O atoms inserted in the basal planes of the two stacking faults. Compare with the experimental image shown in Fig. 8.

Acknowledgements

The authors would like to thank the Aérospatiale company (Division Systèmes Stratégiques et Spatiaux, 33165, Saint-Médard-en-Jalles, France), which partly supported this work, and also Mr S. Abaïdia, for his efficient help in the EXELFS studies.

References

1. Armas, B. & Combescure, C., Chemical vapor deposition of Si_3N_4 and AlN on carbon fibers. In *Proc. 10th Int. Conf. on CVD*, ed. G. W. Cullen & J. M. Blocher. The Electrochem. Society, Pennington, 1987, pp. 1060–9.
2. Aspar, B., Contribution à l'étude du système Al–O–N par dépôt chimique en phase gazeuse. *Thèse de Doctorat*, Université de Montpellier II, 1991.
3. Pauleau, Y., Hantzpergue, J. J. & Remy, J. C., Les couches minces de nitrure d'aluminium. *Bull. Soc. Chim. France*, **5–6** (1979) I-199–I-214.
4. Kilaas, R. & O'Keefe, M. A., The design of a computer system for image simulation and image processing of high resolution electron micrographs. In *Computer Simulation of Electron Microscope Diffraction and Images*, ed. W. Krakow & M. O'Keefe. TMMS, Warrendale, 1989, pp. 171–83.
5. Tang, D. & Dorignac, D., The calculation of scattering factors in HREM image simulation. *Acta Cryst. A*, **50** (1994) 45–52.
6. Serin, V., Zanchi, G. & Sévely, J., EXELFS as a structural tool for studies of low-*Z* elements. *Microsc. Microanal. Microstruct.*, **3** (1992) 201–12.
7. Wyckoff, R. W. G., *Crystal Structures*, 2nd edn, Vol. 1. Interscience Publishers, NY, 1965, pp. 111–20.
8. Egerton, R. F., The range of validity of EELS microanalysis formulae. *Ultramicroscopy*, **6** (1981) 297–300.
9. Hagège, S. & Ishida, Y., On the structure of faulted interfaces in aluminium nitride ceramics. *Phil. Mag. A*, **63**(2) (1991) 241–58.
10. Aspar, B., Rodriguez-Clemente, R., Figueras, A., Armas, B. & Combescure, C., Influence of the experimental conditions on the morphology of CVD AlN films. *J. Cryst. Growth*, **129** (1993) 56–66.
11. Callahan, D. L. & Thomas, G., Impurity distribution in polycrystalline aluminium nitride ceramics. *J. Am. Ceram. Soc.*, **73**(7) (1990) 2167–70.
12. Youngman, R. A., Harris, J. H., Labun, P. A., Graham, R. J. & Weiss, J. K., Inversion domain boundaries and oxygen accommodation in aluminium nitride. *Mat. Res. Soc. Symp. Proc.*, **167** (1990) 271–6.
13. McCartney, M. R., Youngman, R. A. & Teller, R. G., High-resolution electron microscopy of planar inversion domain boundaries in aluminium nitride. *Ultramicroscopy*, **40** (1992) 291–9.
14. Dorignac, D., Mazel, A., Sévely, J., Armas, B., Combescure, C., Aspar, B. & Figueras, A., HREM observation of ceramic layers obtained by LPCVD. In *Electron Microscopy*, ed. Eurem. Secr. Univ., Granada, Vol. 1, 1992, pp. 503–4. Dorignac, D., Mazel, A., Tang, D. & Marti, P., in preparation.